Inorg. Chem. **2007**, *46*, 1369–1378

Synthesis of $[F_3S{\equiv}NXeF][AsF_6]$ and Structural Study by Multi-NMR and Raman Spectroscopy, Electronic Structure Calculations, and X-ray Crystallography

Gregory L. Smith, Hélène P. A. Mercier, and Gary J. Schrobilgen*

Department of Chemistry, McMaster University, Hamilton, Ontario L8S 4M1, Canada

Received October 3, 2006

The salt, $[F_3S{\equiv}NXeF][AsF_6]$, has been synthesized by the reaction of $[XeF][AsF_6]$ with liquid $N{\equiv}SF_3$ at −20 °C. The Xe–N bonded cation provides a rare example of xenon bound to an inorganic nitrogen base in which nitrogen is formally sp-hybridized. The $F_3S{\equiv}NXeF^+$ cation was characterized by Raman spectroscopy at −150 °C and by ^{129}Xe, ^{19}F, and ^{14}N NMR spectroscopy in HF solution at −20 °C and in BrF_5 solution at −60 °C. Colorless $[F_3S{\equiv}NXeF][AsF_6]$ was crystallized from HF solvent at −45 °C, and its low-temperature X-ray crystal structure was determined. The Xe–N bond is among the longest Xe–N bonds known (2.236(4) Å), whereas the Xe–F bond length (1.938(3) Å) is significantly shorter than that of XeF_2 but longer than in XeF^+ salts. The Xe–F and Xe–N bond lengths are similar to those of $HC{\equiv}NXeF^+$, placing it among the most ionic Xe–N bonds known. The nonlinear Xe–N–S angle (142.6(3)°) contrasts with the linear angle predicted by electronic structure calculations and is attributed to close N···F contacts within the crystallographic unit cell. Electronic structure calculations at the MP2 and DFT levels of theory were used to calculate the gas-phase geometries, charges, bond orders, and valencies of $F_3S{\equiv}NXeF^+$ and to assign vibrational frequencies. The calculated small energy difference (7.9 kJ mol^{-1}) between bent and linear Xe–N–S angles also indicates that the bent geometry is likely the result of crystal packing. The structural studies, natural bond orbital analyses, and calculated gas-phase dissociation enthalpies reveal that $F_3S{\equiv}NXeF^+$ is among the weakest donor–acceptor adducts of XeF^+ with an Xe–N donor–acceptor interaction that is very similar to that of $HC{\equiv}NXeF^+$, but considerably stronger than that of $F_3S{\equiv}NAsF_5$. Despite the low dissociation enthalpy of the donor–acceptor bond in $F_3S{\equiv}NXeF^+$, ^{129}Xe, ^{19}F, and ^{14}N NMR studies reveal that the $F_3S{\equiv}NXeF^+$ cation is nonlabile at low temperatures in HF and BrF_5 solvents.

Introduction

The first example of xenon bonded to nitrogen, $FXeN(SO_2F)_2$, was synthesized[1] and characterized in the solid state by Raman[2,3] and EPR spectroscopy,[2] by a single-crystal X-ray structure determination,[3] and by solution ^{19}F,[2,3] ^{15}N,[3] and ^{129}Xe[2,3] NMR spectroscopy. Other imidodisulfurylfluoride species containing Xe(II)−N bonds have since been characterized by multi-NMR and Raman spectroscopy, and include $Xe[N(SO_2F)_2]_2$,[2,4] $F[XeN(SO_2F)_2]_2^+$,[2,4,5] $XeN(SO_2F)_2^+$,[5] and $Xe[N(SO_2CF_3)_2]_2$.[6] Additionally, $XeN(SO_2F)_2^+Sb_3F_{16}^-$ was also characterized by a single-crystal X-ray structure determination.[5] In these species, xenon is bonded to sp^2-hybridized nitrogen atoms which derive their stabilities from the high electronegativity[1,2,4−7] and oxidative resistance of the imidodisulfurylfluoride ligand. Most recently, the synthesis and detailed structural characterization of $[F_5TeN(H)Xe][AsF_6]$, the first example of a noble gas bonded to a formally sp^3-hybridized nitrogen center, has been reported from this laboratory.[8]

* To whom correspondence should be addressed. E-mail: schrobil@mcmaster.ca.

(1) LeBlond, R. D.; DesMarteau, D. D. *J. Chem. Soc. Chem. Commun.* **1974**, 555−556.
(2) DesMarteau, D. D.; LeBlond, R. D.; Hossain, S. F.; Nothe, D. *J. Am. Chem. Soc.* **1981**, *103*, 7734−7739.
(3) Sawyer, J. F.; Schrobilgen, G. J.; Sutherland, S. J. *Inorg. Chem.* **1982**, *21*, 4064−4072.
(4) Schumacher, G. A.; Schrobilgen, G. J. *Inorg. Chem.* **1983**, *22*, 2178−2183.
(5) Faggiani, R.; Kennepohl, D. K.; Lock, C. J. L.; Schrobilgen, G. J. *Inorg. Chem.* **1986**, *25*, 563−571.
(6) Foropoulos, J. J.; DesMarteau, D. D. *J. Am. Chem. Soc.* **1982**, *104*, 4260−4261.
(7) Sawyer, J. F.; Schrobilgen, G. J.; Sutherland, S. J. *J. Chem. Soc. Chem. Commun.* **1982**, 210−211.
(8) Fir, B. A.; Whalen, J. M.; Mercier, H. P. A.; Dixon, D. A.; Schrobilgen, G. J. *Inorg. Chem.* **2006**, *45*, 1978−1996.

10.1021/ic061899+ CCC: $37.00
Published on Web 01/26/2007

The Lewis acidity of the XeF^+ cation, as seen from the propensity of XeF^+ to form fluorine bridges with the counteranions of its salts,[9] has been exploited in this laboratory to form Xe(II)−N bonded cations by the reaction of oxidatively resistant electron pair donors with XeF^+.[10] Reactions of XeF^+ with neutral organic nitrogen bases in HF, or XeF_2 with protonated nitrogen base salts in BrF_5, accompanied by HF elimination, have led to cations in which XeF^+ is bonded to formally sp- and sp^2-hybridized nitrogen centers. These include hydrogen cyanide,[11,12] alkylnitriles,[11] pentafluorobenzenenitrile,[11] perfluoroalkylnitriles,[11,13] perfluoropyridines,[14] and *s*-trifluorotriazine.[13] With the exception of the *s*-trifluorotriazine cation, $s\text{-}C_3F_3N_2NXeF^+$, all of the cations decompose below room temperature. The krypton(II) cations, $HC{\equiv}NKrF^{+}$[15] and $R_FC{\equiv}NKrF^+$ ($R_F = CF_3$, C_2F_5, $n\text{-}C_3F_7$),[13] characterized in this laboratory as the AsF_6^- salts, are unstable above ca. −50 °C.

The basicity of $N{\equiv}SF_3$ was previously demonstrated by reaction of $N{\equiv}SF_3$ with BF_3, AsF_5, and SbF_5 in SO_2 to give the Lewis acid−base adducts, $F_3S{\equiv}NBF_3$,[16,17] $F_3S{\equiv}NAsF_5$,[18,19] and $F_3S{\equiv}NSbF_5$[18] and by the formation of $[(CF_3)_nSF_{3-n}{\cdot}N{\equiv}SF_3][AsF_6]$[20] and transition metal complexes,[19,21−26] e.g., $[M(N{\equiv}SF_3)_4][AsF_6]_2$ (M = Mn, Fe, Co Ni, Cu).[22] In view of the established Lewis basicity and anticipated resistance to oxidation (first adiabatic ionization potential, 12.50 eV[27]) of $N{\equiv}SF_3$, its reaction with XeF^+ was investigated in the present paper, providing the synthesis and detailed structural characterization of a rare example of a noble-gas compound in which the noble-gas atom is bonded to an inorganic sp-hybridized nitrogen center.

Results and Discussion

Synthesis of $[F_3S{\equiv}NXeF][AsF_6]$. Thiazyl trifluoride was synthesized as previously described.[28] The salt, $[F_3S{\equiv}NXeF][AsF_6]$, was synthesized by reaction of $[XeF][AsF_6]$ and liquid $N{\equiv}SF_3$ at −25 to −15 °C for ca. 6 h according to eq 1, forming a colorless, microcrystalline solid which was identified by Raman spectroscopy at −150 °C.

$$N{\equiv}SF_3 + [XeF][AsF_6] \xrightarrow[N{\equiv}SF_3]{-25\text{ to }-15\ ^\circ C} [F_3S{\equiv}NXeF][AsF_6] \quad (1)$$

Table 1. Summary of Crystal Data and Refinement Results for $[F_3S{\equiv}NXeF][AsF_6]$

empirical formula	$F_{10}SNXeAs$
space group (No.)	*Pbca* (61)
a (Å)	8.7844(3)
b (Å)	12.3857(4)
c (Å)	16.2550(5)
V (Å^3)	1768.56(5)
molecules/unit cell	8
mol wt (g mol^{-1})	442.29
calcd density (g cm^{-3})	3.322
T (°C)	−173
μ(mm^{-1})	7.97
wavelength (Å)	0.71073
final agreement factors[a]	$R_1 = 0.0438$
	$wR_2 = 0.0679$

[a] R_1 is defined as $\sum ||F_o| - |F_c||/\sum|F_o|$ for $I > 2\sigma(I)$; wR_2 is defined as $[\sum[w(F_o^2 - F_c^2)^2]/\sum w(F_o^2)^2]^{1/2}$ for $I > 2\sigma(I)$.

X-ray Crystal Structure of $[F_3S{\equiv}NXeF][AsF_6]$. A summary of the refinement results and other crystallographic information is provided in Table 1. Important bond lengths and angles for $[F_3S{\equiv}NXeF][AsF_6]$ are listed in Table 2 along with calculated values for the $F_3S{\equiv}NXeF^+$ cation.

The structure of $[F_3S{\equiv}NXeF][AsF_6]$ (Figure 1a) consists of well-separated $F_3S{\equiv}NXeF^+$ cations and AsF_6^- anions. The anion shows no significant distortion from octahedral geometry, with As−F bonds ranging from 1.711(3) to 1.718(3) Å, in good agreement with previously reported values.[8,29] The Xe−N and Xe−F bond lengths, (2.236(4) and (1.938(3) Å), are equal, within experimental error, to those in $[HC{\equiv}NXeF][AsF_6]$ (2.235(3) and 1.936(2) Å)[30] and are comparable to those observed in $[CH_3C{\equiv}NXeF][AsF_6]{\cdot}HF$ (2.179(7) and 1.947(5) Å)[30] and $[(CH_3)_3CC{\equiv}NXeF][AsF_6]$ (2.212(4) and 1.952(3) Å).[30] The Xe−N bond in $F_3S{\equiv}NXeF^+$ is significantly shorter than the Xe−N bonds in $CH_3C{\equiv}N{\cdot}{\cdot}{\cdot}XeC_6F_5^+$ (2.681(8) Å)[31] and $[2,6\text{-}C_5H_3F_2N{\cdot}{\cdot}{\cdot}XeC_6F_5][AsF_6]$ (2.694(5) Å).[32] The Xe−F bond length of $F_3S{\equiv}NXeF^+$ is significantly longer than the terminal Xe−F bond length in $[XeF][AsF_6]$ (1.888(3),[33] 1.873(6) Å[34]) and other XeF^+ salts[33,35] but shorter than those in XeF_2 (2.010(6),[36] 1.999(4) Å[33]). The relationship between the relative strength of the donor−acceptor interactions in XeF^+ salts, i.e., $FXe^+{\cdot}{\cdot}{\cdot}F{-}MF_5^-$ and $FXe^+{\cdot}{\cdot}{\cdot}F{-}M_2F_{10}^-$, and Xe−F bond

(9) Selig, H.; Holloway, J. H. In *Topics in Current Chemistry*; Bosche, F. L., Ed.; Springer-Verlag: Berlin, 1984; Vol. 124, pp 33−90.
(10) Schrobilgen, G. J. In *Synthetic Fluorine Chemistry*; Olah, G. A.; Chambers, R. D., Prakash, G. K. S., Eds.; John Wiley and Sons: New York, 1992; pp 1−30.
(11) Emara, A. A. A.; Schrobilgen, G. J. *J. Chem. Soc. Chem. Commun.* **1987**, 1644−1646.
(12) Emara, A. A. A.; Schrobilgen, G. J. *Inorg. Chem.* **1992**, *31*, 1323−1332.
(13) Schrobilgen, G. J. *J. Chem. Soc. Chem. Commun.* **1988**, 1506−1508.
(14) Emara, A. A. A.; Schrobilgen, G. J. *J. Chem. Soc. Chem. Commun.* **1988**, 257−259.
(15) Schrobilgen, G. J. *J. Chem. Soc. Chem. Commun.* **1988**, 863−865.
(16) Glemser, O.; Richert, H. *Z. Anorg. Allg. Chem.* **1961**, *307*, 313−327.
(17) Muller, A.; Glemser, O.; Scherf, K. *Chem. Ber.* **1966**, *99*, 3568−3571.
(18) Glemser, O.; Koch, W. *Anales. Asoc. Quim. Argentina* **1971**, *59*, 143−148.
(19) Glemser, O.; Mews, R. *Angew. Chem., Int. Ed. Engl.* **1980**, *19*, 883−899.
(20) Erhart, M.; Mews, R. *Z. Anorg. Allg. Chem.* **1992**, *615*, 117−122.
(21) Buss, B.; Clegg, W.; Hartmann, G.; Jones, P. G.; Mews, R.; Noltemeyer, M.; Sheldrick, G. M. *J. Chem. Soc. Dalton Trans.* **1981**, 61−63.
(22) Mews, R. *J. Chem. Soc. Chem. Commun.* **1979**, 278−279.
(23) Mews, R.; Glemser, O. *Angew. Chem., Int. Ed. Engl.* **1975**, *14*, 186−187.
(24) Behrens, U.; Hoppenheit, R.; Isenberg, W.; Lork, E.; Petersen, J.; Mews, R. *Z. Naturforsch.* **1994**, *49b*, 238−242.
(25) Schnepel, F. M.; Mews, R.; Glemser, O. *J. Mol. Struct.* **1980**, *60*, 89−92.
(26) Behrens, U.; Lork, E.; Petersen, J.; Waterfeld, A.; Mews, R. *Z. Anorg. Allg. Chem.* **1997**, *623*, 1518−1524.
(27) Beach, D., B.; Jolly, W. L.; Mews, R.; Waterfeld, A. *Inorg. Chem.* **1984**, *23*, 4080−4084.
(28) Mews, R.; Keller, K.; Glemser, O. *Inorg. Synth.* **1986**, *24*, 12−17.
(29) Fir, B. A.; Gerken, M.; Pointner, B. E.; Mercier, H. P. A.; Dixon, D. A.; Schrobilgen, G. J. *J. Fluorine Chem.* **2000**, *105*, 159−167.
(30) Fir, B. A.; Mercier, H. P. A.; Schrobilgen, G. J.; Suontamo, R. J.; Emara, A. A. A. to be submitted for publication.
(31) Frohn, H.-J.; Jakobs, S.; Henkel, G. *Angew. Chem., Int. Ed. Engl.* **1989**, *28*, 1506−1507.
(32) Frohn, H. J.; Schroer, T.; Henkel, G. *Z. Naturforsch.* **1995**, *50b*, 1799−1810.

Table 2. Experimental Geometry for $[F_3S{\equiv}NXeF][AsF_6]$ and Calculated Geometries for $F_3S{\equiv}NXeF^+$, $N{\equiv}SF_3$, and XeF^+

Bond Lengths (Å)

		calcd[a]					
		$F_3S{\equiv}NXeF^+$ (C_1)		$N{\equiv}SF_3$ (C_{3v})		XeF^+ ($C_{\infty v}$)	
	exptl	MP2	SVWN	MP2	SVWN	MP2	SVWN
Xe(1)−N(1)	2.236(4)	2.295	2.242				
Xe(1)−F(1)	1.938(3)	1.916	1.933			1.874	1.878
S(1)−N(1)	1.397(5)	1.418	1.416	1.437	1.449		
S(1)−F(2)	1.503(3)	1.528	1.532	1.574	1.616		
S(1)−F(3)	1.503(3)	1.528	1.532	1.574	1.616		
S(1)−F(4)	1.496(3)	1.528	1.532	1.574	1.616		
As(1)−F(5)	1.713(3)						
As(1)−F(6)	1.715(3)						
As(1)−F(7)	1.711(3)						
As(1)−F(8)	1.716(3)						
As(1)−F(9)	1.717(3)						
As(1)−F(10)	1.718(3)						
N(1)···F(1A)	3.097(6)						
N(1)···F(10A)	3.076(5)						
N(1)···F(6B)	3.133(5)						
N(1)···F(5A)	3.201(6)						

Bond Angles (°)

		calcd[a]			
		$F_3S{\equiv}NXeF^+$ (C_1)		$N{\equiv}SF_3$ (C_{3v})	
	exptl	MP2	SVWN	MP2	SVWN
F(1)−Xe(1)−N(3)	179.6(2)	180.0	180.0		
Xe(1)−N(1)−S(3)	142.6(3)	180.0	180.0		
N(1)−S(1)−F(2)	115.2(2)	120.3	120.0	123.8	123.0
N(1)−S(1)−F(3)	120.7(2)	120.3	120.0	123.8	123.0
N(1)−S(1)−F(4)	123.4(2)	120.3	120.0	123.8	123.0
F(2)−S(1)−F(3)	97.1(2)				
F(2)−S(1)−F(4)	97.7(2)				
F(3)−S(1)−F(4)	97.3(2)				
F(5)−As(1)−F(6)	179.1(2)				
F(5)−As(1)−F(7)	90.3(2)				
F(5)−As(1)−F(8)	89.7(2)				
F(5)−As(1)−F(9)	90.0(2)				
F(5)−As(1)−F(10)	90.2(2)				
F(6)−As(1)−F(7)	89.9(2)				
F(6)−As(1)−F(8)	89.4(2)				
F(6)−As(1)−F(9)	90.8(2)				
F(6)−As(1)−F(10)	89.6(2)				
F(7)−As(1)−F(8)	90.0(2)				
F(7)−As(1)−F(9)	90.8(2)				
F(7)−As(1)−F(10)	179.4(2)				
F(8)−As(1)−F(9)	179.2(2)				
F(8)−As(1)−F(10)	89.6(2)				
F(9)−As(1)−F(10)	89.6(2)				

[a] (SDB-)cc-pVTZ basis set.

length is well established and leads to Xe−F bond strengthening with decreasing fluoro-basicity and a corresponding increase in ν(XeF).[37,38] Of the crystallographically characterized N−Xe−F bonded cations having formal sp-hybridization at N, the Xe−N and Xe−F bond lengths in the $F_3S{\equiv}NXeF^+$ cation are most similar to those of $HC{\equiv}NXeF^+$[30] and to the terminal Xe−F bond length in

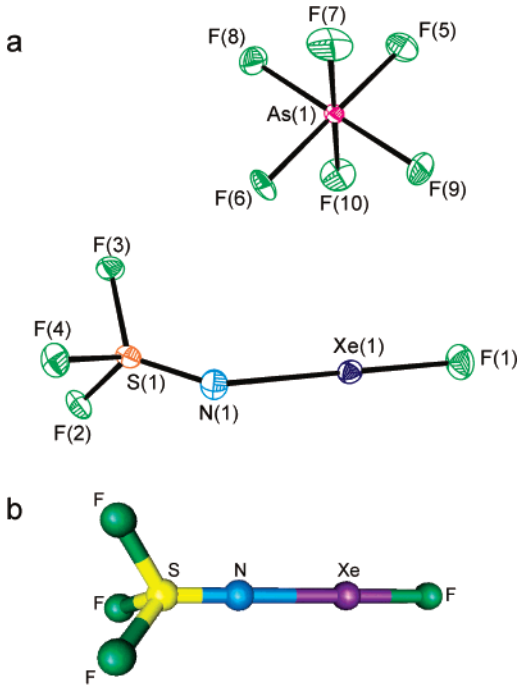

Figure 1. (a) X-ray crystal structure of $[F_3S{\equiv}NXeF][AsF_6]$; thermal ellipsoids are shown at the 50% probability level. (b) Calculated geometry of the $F_3S{\equiv}NXeF^+$ cation. The atom numbering scheme corresponds to that given in Table 2 where the values of experimental and calculated geometric parameters are provided.

$[Xe_2F_3][AsF_6]$ (1.90(3),[39] 1.915(8) Å[29]), thus placing the XeF^+ adducts of $N{\equiv}SF_3$ and $HC{\equiv}N$ toward the most ionic end of the scale.

The S−N and S−F bonds of $[F_3S{\equiv}NXeF][AsF_6]$ (1.397(5) and 1.503(3) Å) are shorter than those in $N{\equiv}SF_3$ (1.416(3) and 1.552(3) Å).[40] Similar bond length contractions occur in other $N{\equiv}SF_3$ complexes, i.e., $F_3S{\equiv}NAsF_5$ (1.383 and 1.439 Å),[19] $[Mn(N{\equiv}SF_3)_4][AsF_6]_2$ (1.365(11) and 1.506(5) Å),[21] $[Zn(N{\equiv}SF_3)_4][AsF_6]_2$ (1.365(7) and 1.496(6) Å),[24] $[Re(CO)_5N{\equiv}SF_3][AsF_6]$ (1.384(14) and 1.499(10) Å),[25] and $[CpFe(CO)_2N{\equiv}SF_3][AsF_6]$ (1.376(3) and 1.515(3) Å).[26]

Although quantum mechanical calculations predict a linear structure (Figure 1b, also see Computational Results), the Xe−N−S angle (142.6(3)°) is significantly more distorted from linearity than the Xe−N−C angles in the crystal structures of $[HC{\equiv}NXeF][AsF_6]$ (177.7(3)°),[30] $[CH_3C{\equiv}NXeF][AsF_6]{\cdot}HF$ (175.0(8)°),[30] and $[(CH_3)_3CC{\equiv}NXeF][AsF_6]$ (166.9(4)°),[30] however, no explanations were given. Other bent E−N−C (E = In, Tl, Sn, Pb) arrangements have been encountered in the solid state.[41−44] In the present instance, the bent Xe−N−S angle

(33) Elliott, H. S. A.; Jenkins, H. D. B.; Lehmann, J. F.; Mercier, H. P. A.; Schrobilgen, G. J. to be submitted for publication.
(34) Zalkin, A.; Ward, D. L.; Biagioni, R. N.; Templeton, D. H.; Bartlett, N. *Inorg. Chem.* **1978**, *17*, 1318−1322.
(35) Bartlett, N.; Gennis, M.; Gibler, D. D.; Morrell, B. K.; Zalkin, A. *Inorg. Chem.* **1973**, *12*, 1717−1721.
(36) Burns, J. H.; Ellison, R. D.; Levy, H. A. *Acta. Crystallogr.* **1965**, *18*, 11−16.
(37) Gillespie, R. J.; Landa, B. *Inorg. Chem.* **1973**, *12*, 1383−1388.
(38) Gillespie, R. J.; Martin, D.; Schrobilgen, G. J. *J. Chem. Soc. Dalton Trans.* **1980**, 1898−1903.
(39) Bartlett, N.; DeBoer, B. G.; Hollander, F. J.; Sladky, F. O.; Templeton, D. H.; Zalkin, A. *Inorg. Chem.* **1974**, *13*, 780−785.
(40) Kirchhoff, W. H.; Wilson, E. B., Jr. *J. Am. Chem. Soc.* **1962**, *84*, 334−336.
(41) Lu, J.; Harrison, W. T. A.; Jacobson, A. J. *Angew. Chem., Int. Ed. Engl.* **1995**, *34*, 2557−2559.
(42) Connelly, N. G.; Hicks, O. M.; Lewis, G. R.; Moreno, M. T.; Orpen, A. G. *J. Chem. Soc. Dalton Trans.* **1998**, 1913−1917.
(43) Werner, B.; Kräuter, T.; Neumüller, B. *Z. Anorg. Allg. Chem.* **1995**, *621*, 346−358.
(44) Behrens, U.; Brimah, A. K.; Soliman, T. M.; Fischer, R. D.; Apperly, D. C.; Davies, N. A.; Harris, R. K. *Organometallics.* **1992**, *11*, 1718−1726.

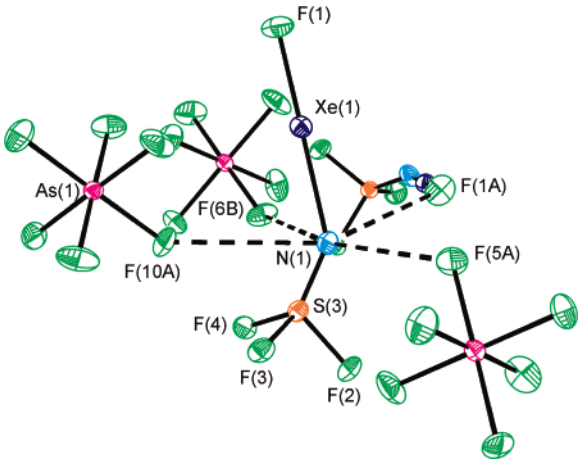

Figure 2. View of the $F_3S{\equiv}NXeF^+$ cation showing the closest N···F contacts with three neighboring AsF_6^- anions and the fluorine on xenon of a neighboring $F_3S{\equiv}NXeF^+$ cation.

appears to result from several close N···F contacts within the crystal lattice, three from anions (3.076(5), 3.133(5), 3.201(6) Å) and one from the fluorine ligand bonded to xenon (3.097(6) Å) in a neighboring $F_3S{\equiv}NXeF^+$ cation. These contacts are at the limit of the sum of nitrogen and fluorine van der Waals radii (3.02 Å),[45] and form a distorted square planar arrangement about nitrogen (Figure 2) with the cation bent toward the longest, most open edge.

The N−S−F and F−S−F angles in $[F_3S{\equiv}NXeF][AsF_6]$ average 119.8(2)° and 97.4(2)°, respectively, comprising a distorted tetrahedral arrangement about sulfur that is similar to those of $N{\equiv}SF_3$ (122.4(8)°[46] and 94.0(3)°[40]), $F_3S{\equiv}NAsF_5$ (122.2° and 94.3°),[19] and $[CpFe(CO)_2N{\equiv}SF_3][AsF_6]$ (120.9(2)° and 96.0(2)°).[26]

NMR Spectroscopy. The ^{14}N, ^{19}F, and ^{129}Xe NMR parameters for $[F_3S{\equiv}NXeF][AsF_6]$ recorded in anhydrous HF solvent at −20 °C and BrF_5 solvent at −60 °C (NMR parameters obtained from BrF_5 solutions are given in parentheses) are listed in Table 3.

The ^{19}F spectrum consists of two singlets at 51.2 (53.3) and −185.5 (−180.5) ppm, corresponding to the fluorine-on-sulfur (Figure 3a) and fluorine-on-xenon (Figure 3b) environments, respectively. The latter singlet is accompanied by natural abundance ^{129}Xe (26.44%) satellites resulting from $^1J(^{129}Xe{-}^{19}F) = 6265$ (6248) Hz. The $^4J(^{19}F_{Xe}{-}^{19}F_S)$ coupling cannot be observed in HF solvent, which may be a consequence of line broadening (F-on-S, $\Delta\nu_{1/2} = 47$ Hz and F-on-Xe, $\Delta\nu_{1/2} = 150$ Hz) arising from slow chemical exchange between HF and $F_3S{\equiv}NXeF^+$ (eq 2). A diminished

$$F_3S{\equiv}NXeF^+ + 2HF \rightleftharpoons XeF_2 + N{\equiv}SF_3 + H_2F^+ \quad (2)$$

fluorine exchange rate in BrF_5 and a greatly enhanced rate of quadrupolar relaxation of residual $^2J(^{19}F_S{-}^{14}N)$ and $^2J(^{19}F_{Xe}{-}^{14}N)$ couplings that result from the higher viscosity of BrF_5 at −60 °C are apparently responsible for the line narrowing[47] that permits observation of the $^4J(^{19}F_{Xe}{-}^{19}F_S)$ coupling (doublet, 15.1 Hz, $\Delta\nu_{1/2} = 26$ Hz) on the F-on-S environment (vide infra). The anticipated 1:3:3:1 quartet corresponding to the F-on-Xe environment could only be partially resolved in BrF_5 solvent ($\Delta\nu_{1/2} = 45$ Hz).

The ^{129}Xe spectrum (Figure 4) consists of a doublet arising from $^1J(^{129}Xe{-}^{19}F) = 6265$ (6248) Hz which, in turn, is split into a 1:1:1 triplet ($^1J(^{129}Xe{-}^{14}N) = 350$ Hz) in anhydrous HF. The outer transitions of the triplets are broader than the central transition owing to partial quadrupolar relaxation of ^{14}N ($I = 1$) in the presence of the small electric field gradient at ^{14}N in this axially symmetric cation. Similar $^1J(^{129}Xe{-}^{14}N)$ couplings have been observed for the $HC{\equiv}N$ and alkyl nitrile adducts of XeF^+ when recorded in HF solvent (cf. $HC{\equiv}NXeF^+$, $^1J(^{129}Xe{-}^{19}F) = 6161$ Hz and $^1J(^{129}Xe{-}^{14}N) = 332$ Hz at −10 °C).[30] The ^{129}Xe NMR chemical shift, $\delta(^{129}Xe) = -1652$ (−1661) ppm, is consistent with that expected for an Xe−F moiety bound to an sp-hybridized nitrogen (cf. $HC{\equiv}NXeF^+$, $\delta(^{129}Xe) = 1552$ (−1570) ppm in HF (BrF_5) solvent at −10 (−50) °C).[30] When the ^{129}Xe NMR spectrum was recorded in BrF_5 solvent, the $^1J(^{129}Xe{-}^{14}N)$ coupling was quadrupole collapsed to a doublet corresponding to $^1J(^{129}Xe{-}^{19}F)$. Complete collapse of the $^1J(^{129}Xe{-}^{14}N)$ coupling in BrF_5 solvent is attributed to fast quadrupolar relaxation of ^{14}N that is mainly a consequence of the high viscosity[47] of BrF_5 at −60 °C. The ^{14}N spectrum of $F_3S{\equiv}NXeF^+$ recorded in HF at −20 °C consisted of a quadrupole broadened resonance ($\Delta\nu_{1/2} = 750$ Hz) at −278.0 ppm, which obscured the expected ^{129}Xe satellites.

Other than an early ^{19}F NMR study of $N{\equiv}SF_3$, which only reported the $^2J(^{19}F{-}^{14}N)$ coupling constant (27 Hz),[48] the NMR spectroscopic characterization of $N{\equiv}SF_3$ appears to be incomplete. In the present study, the following NMR parameters for $N{\equiv}SF_3$ have been determined in SO_2ClF solvent at 30 °C: $\delta(^{19}F) = 68.3$ ppm, $\delta(^{14}N) = -245.8$ ppm, $^1J(^{19}F{-}^{14}N) = 26.6$ Hz, $^1\Delta^{19}F^{(34/32)}S = 0.058$ ppm. The ^{19}F and ^{14}N chemical shifts of $N{\equiv}SF_3$ and $F_3S{\equiv}NXeF^+$ have been measured in different solvents at different temperatures because $N{\equiv}SF_3$ undergoes HF solvolysis to yield F_5SNH_2[49] and because $[F_3S{\equiv}NXeF][AsF_6]$ is insoluble in SO_2ClF. The complexation shifts, $\delta(^{19}F_S)_{F_3S{\equiv}NXeF^+} - \delta(^{19}F_S)_{N{\equiv}SF_3} = -17.1$ [−15.0] ppm and $\delta(^{14}N)_{F_3S{\equiv}NXeF^+} - \delta(^{14}N)_{N{\equiv}SF_3} = -32.2$ ppm, indicate that both the $^{19}F_S$ and ^{14}N environments are more shielded in the cation. The individual shielding tensors that contribute to the isotropic shielding would need to be determined for a fuller understanding of the complexation shifts. It is noteworthy, however, that the increased shielding of ^{14}N in $F_3S{\equiv}NXeF^+$ parallels its increased charge and valency, whereas the charges of the more highly shielded fluorine ligands bonded to sulfur have diminished, but their valencies have also increased relative to those of $N{\equiv}SF_3$ (see Computational Results).

(45) Bondi, A. *J. Phys. Chem.* **1964**, *68*, 441−451.
(46) Calculated from the published (ref 40) bond lengths and F−S−F angles of $N{\equiv}SF_3$ determined from microwave spectroscopy.
(47) Sanders, J. C. P.; Schrobilgen, G. J. In *A Methodological Approach to Multinuclear NMR in Liquids and Solids-Chemical Applications; NATO Advanced Study Institute, Magnetic Resonance*; Granger, P., Harris, R. K., Eds.; Kluwer Academic Publishers: Dordrecht, 1990; Chapter 11, pp 157−186.
(48) Richert, H.; Glemser, O. *Z. Anorg. Allg. Chem.* **1961**, *307*, 328−344.
(49) Clifford, A. F.; Duncan, L. C. *Inorg. Chem.* **1966**, *5*, 692−693.

Table 3. NMR Chemical Shifts and Spin−Spin Coupling Constants for $[F_3S{\equiv}NXeF][AsF_6]$[a]

	chemical shifts, ppm			coupling constants, Hz		
species	$\delta(^{129}Xe)$	$\delta(^{19}F)$	$\delta(^{14}N)$	$^1J(^{129}Xe-^{19}F)$	$^1J(^{129}Xe-^{14}N)$	$^nJ(^{19}F-^{19}F)$
$F_3S{\equiv}NXeF^+$ [b]	−1652 (−1661)	−185.5 (−180.5), F_{Xe} 51.2 (53.3), F_S	−278.0	6265 (6248)	350	(15.1), $n = 4$
AsF_6^- [c]		−69 (−62)				
HF		−197				
BrF_5 [d]		(136.4), F_{eq} (274.4), F_{ax}				(77.0), $n = 2$

[a] The values in parentheses have been measured in BrF_5 at −60 °C; all other values have been measured in HF at −20 °C. The secondary isotope effect of $^{32/34}S$ on ^{19}F, $^1\Delta^{19}F(^{34/32}S) = -0.066$ ppm, was observed in both HF and BrF_5 solvents. [b] The fluorines bonded to Xe and S are denoted by F_{Xe} and F_S, respectively. [c] The ^{19}F resonance of AsF_6^- was a broad, saddle-shaped feature, $\Delta\nu_{1/2} = 2860$ (2500) Hz, as a result of partial quadrupole-collapse of the $^1J(^{75}As-^{19}F)$ coupling. [d] The axial (quintet) and equatorial (doublet) ^{19}F environments, denoted by F_{ax} and F_{eq}, respectively, exhibited bromine secondary isotope shifts: $^1\Delta^{19}F_{ax}(^{79/81}Br) = -0.012$ ppm and $^1\Delta^{19}F_{eq}(^{79/81}Br) = -0.029$ ppm.

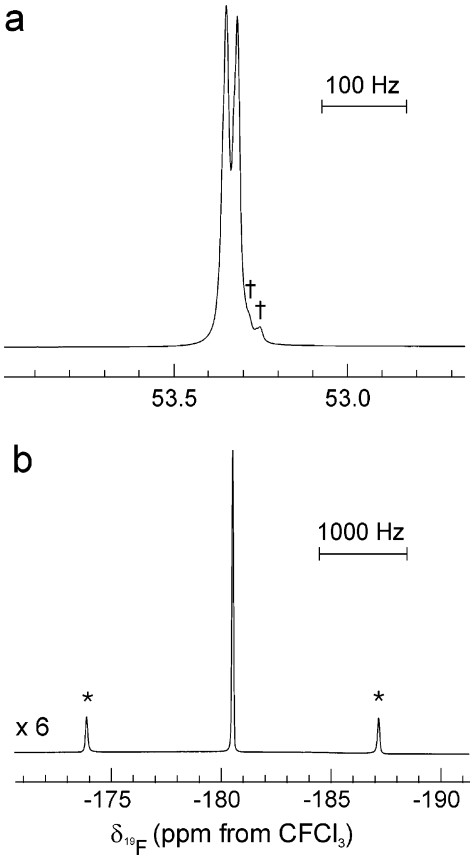

Figure 3. ^{19}F NMR spectrum (470.592 MHz) of $[F_3S{\equiv}NXeF][AsF_6]$ in BrF_5 at −60 °C showing the cation resonances; (a) the F-on-S environment; daggers (†) denote the $^1\Delta^{19}F_S(^{34/32}S)$ secondary isotope shift, and (b) the F-on-Xe environment; asterisks (*) denote ^{129}Xe satellites.

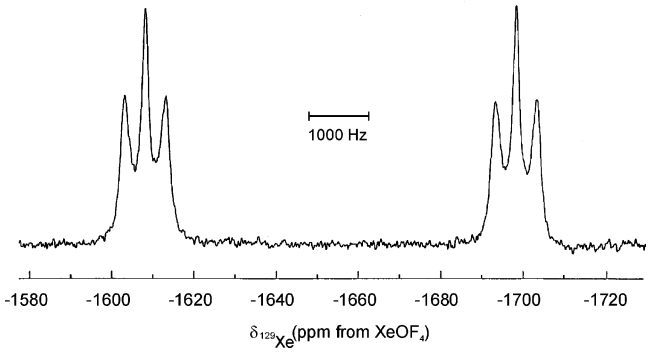

Figure 4. ^{129}Xe NMR spectrum (138.086 MHz) of $[F_3S{\equiv}NXeF][AsF_6]$ in anhydrous HF solvent at −20 °C.

Raman Spectroscopy. The Raman spectrum of $[F_3S{\equiv}NXeF][AsF_6]$ was assigned by comparison with that of solid $N{\equiv}SF_3$, recorded during the course of this study, and previously published vibrational assignments for $N{\equiv}SF_3$[19,48,50,51] and AsF_6^- [8] and by electronic structure calculations (see Computational Results).

The $F_3S{\equiv}NXeF^+$ cation (C_1 symmetry) possesses 15 Raman- and infrared-active fundamental vibrational modes belonging to the A irreducible representations. The 15 vibrational modes of AsF_6^- belong to the irreducible representations $A_{1g} + E_g + T_{2g} + 2T_{1u} + T_{2u}$ under O_h symmetry, where the A_{1g}, E_g, and T_{2g} modes are Raman active and the T_{1u} modes are infrared active. The eight cations and anions occupy C_1 sites in the crystallographic unit cell. Factor-group analyses for the cation and anion are provided in Table S1 and predict that each gas-phase Raman- and infrared-active vibrational mode of $F_3S{\equiv}NXeF^+$ and AsF_6^- is split, as a result of site symmetry lowering, into a maximum of four Raman-active (A_g, B_{1g}, B_{2g}, B_{3g}) and infrared-active (A_u, B_{1u}, B_{2u}, B_{3u}) components. Anion bands, under O_h symmetry, corresponding to the $\nu_1(A_{1g})$, $\nu_2(E_g)$, and $\nu_3(T_{1u})$ modes were split into two components and $\nu_4(T_{1u})$ was split into three components in the experimental spectrum (Figure 5). The cation splittings were only resolved for the vibrational modes associated with the $N{\equiv}SF_3$ group, i.e., the $\delta_s(SF_3)$ mode (four components), the $\nu(SN)$, $\nu_{as}(SF_3)$, and $\nu_s(SF_3)$ modes (three components each), and the $\delta(NSF_2)$ and $\delta_{as}(NSF_3)$ modes (two components each).

Vibrational frequencies calculated at the MP2 and SVWN levels of theory reproduced all the experimental frequency trends, although $\nu(SN)$ and $\nu(XeF)$ are both predicted to be ca. 60 cm^{-1} higher than the experimental frequencies (Table 4).

The XeF stretching mode of $F_3S{\equiv}NXeF^+$ (550 cm^{-1}) is characteristically intense, having a frequency that is intermediate with respect to those of $FXeN(SO_2F)_2$ (506 cm^{-1})[2] and $[XeF][AsF_6]$ (608, 610 cm^{-1}),[52] and very similar to that of $HC{\equiv}NXeF^+$ (561, 569 cm^{-1}).[30] The XeF stretching frequency trend correlates with the Xe−F bond lengths of these species and with donor atom base strength, decreasing

(50) Koeniger, F.; Müller, A.; Glemser, O. *J. Mol. Struct.* **1978**, *46*, 29−34.
(51) Müller, A.; Ruoff, A.; Krebs, B.; Glemser, O.; Koch, W. *Spectrochim. Acta. Part A* **1969**, *25*, 199−205.
(52) This work.

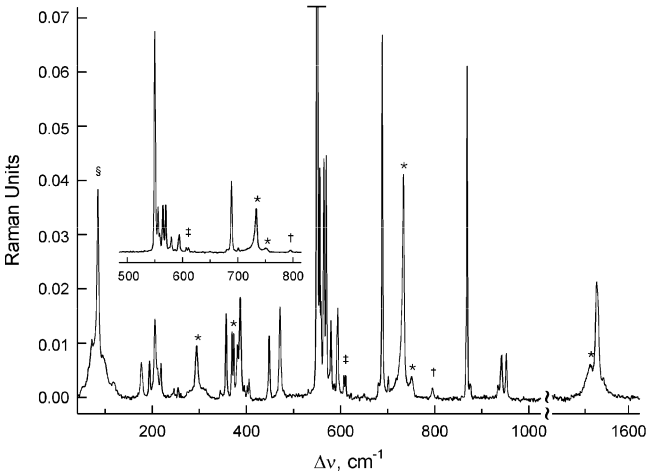

Figure 5. Raman spectrum of $[F_3S{\equiv}NXeF][AsF_6]$ recorded at −150 °C using 1064-nm excitation; the symbols denote FEP sample tube lines (*), $\nu_s(SF_3)$ of unreacted $N{\equiv}SF_3$ (†), ν(XeF) of unreacted [XeF][AsF_6] (‡), and an instrumental artifact (§).

with increasing base strength,[37,53] affirming the highly ionic characters of the Xe−N bonds in $F_3S{\equiv}NXeF^+$ and $HC{\equiv}NXeF^+$. The experimental shift of 59 cm^{-1} of ν(XeF) in $F_3S{\equiv}NXeF^+$ to lower frequency relative to that of [XeF][AsF_6] is in accord with the calculated gas-phase complexation shifts of 55/63 (MP2/SVWN) cm^{-1} for XeF^+ and $F_3S{\equiv}NXeF^+$.

Correspondingly, the ν(XeN) stretch occurs at low frequency and is assigned to the band at 194 cm^{-1}, which is slightly higher than that observed in $(CH_3)_3CC{\equiv}NXeF^+$ (188 cm^{-1})[30] but significantly lower than those observed in $CH_3C{\equiv}NXeF^+$ (280 cm^{-1}),[30] $HC{\equiv}NXeF^+$ (331 cm^{-1}),[30] and $FXeN(SO_2F)_2$ (422 cm^{-1}).[2] The NXeF bend is assigned to the band at 177 cm^{-1}, which is comparable to those of $CH_3C{\equiv}NXeF^+$ (160, 170 cm^{-1})[30] and $HC{\equiv}NXeF^+$ (181 cm^{-1}).[30]

All $N{\equiv}SF_3$ modes of $F_3S{\equiv}NXeF^+$ exhibit complexation shifts to higher frequency relative to those of solid $N{\equiv}SF_3$. The highest frequency mode, assigned to ν(SN), occurs 20 cm^{-1} to higher frequency with respect to that of $N{\equiv}SF_3$ but is much less than the calculated shifts of 116/141 cm^{-1}. The average $\nu_{as}(SF_3)$ and $\nu_s(SF_3)$ frequencies increase 111 (132/173) and 94 (114/132) cm^{-1}, respectively, upon complexation, and the bending modes, $\delta_s(SF_3)$, $\delta(NSF_2)$, and $\delta_{as}(NSF_3)$, shift to higher frequency by 34, 26, and 11 (36/75, 21/31, 8/23) cm^{-1}, respectively. The high-frequency shifts are in accord with the S−N and S−F bond length contractions that result upon adduct formation with XeF^+. Bands below 220 cm^{-1}, which are not otherwise explicitly assigned, are attributed to lattice modes. The lowest frequency mode, torsion about Xe, was calculated at 32/15 cm^{-1}, but could not be observed.

Computational Results. Electronic structure calculations were carried out at the MP2 and DFT (SVWN) levels using cc-pVTZ or (SDB-)cc-pVTZ basis sets for $F_3S{\equiv}NXeF^+$ and XeF^+ to support the vibrational assignments (see Raman Spectroscopy) and to gain insight into the structure and bonding of $F_3S{\equiv}NXeF^+$ (Table 2). The energy-minimized geometries and vibrational frequencies of $N{\equiv}SF_3$ and XeF^+ were also calculated and served as benchmarks. The MP2 calculations provided vibrational frequencies that were in better agreement with the experimental frequencies and better reproduced their trends, while the SVWN calculations (values given in parentheses) provided geometrical parameters that were in better agreement with the experimental values.

(a) Calculated Geometries. Although close to C_{3v} symmetry, both the MP2 and SVWN energy-minimized structures of $F_3S{\equiv}NXeF^+$ had C_1 symmetry. Both levels of theory reproduced the experimentally observed decreases in the S−N and S−F bond lengths upon complex formation with XeF^+, and the Xe−F bond elongation [0.04 (0.06) Å] with respect to that calculated for gas-phase XeF^+. The Xe−N−S angle, found to be bent by low-temperature X-ray diffraction (vide supra), was linear in the calculated geometry. The calculated MP2 energy difference between the experimental bent and calculated linear geometries (7.9 kJ mol^{-1}) indicates that the Xe−N−S angle is very deformable and is most likely the result of crystal lattice packing.

Because the valence electron lone pair on the nitrogen atom of $N{\equiv}SF_3$ is formally sp-hybridized, Xe−N donor−acceptor bond formation directly influences the S−N σ bond by strengthening and shortening this bond through removal of charge density from S. Enhancement of the sulfur positive charge, in turn, leads to shorter, more covalent S−F bonds. This agrees with the trend in the calculated bond lengths for $N{\equiv}SF_3$ and $F_3S{\equiv}NXeF^+$ where the S−N bond shortens by 0.19 (0.33) Å and the S−F bond shortens by 0.46 (0.84) Å upon cation formation.

(b) Charges, Valencies, and Bond Orders. The natural bond orbital (NBO) charges, valencies, and bond orders calculated at the MP2 and SVWN levels of theory (SVWN values are given in parentheses) for $N{\equiv}SF_3$ and $F_3S{\equiv}NXeF^+$ are listed in Table 5. The experimental and calculated contraction of the S−F and S−N bond lengths, elongation of the Xe−F bond, and elongation of the Xe−N bond upon complexation are corroborated by the NBO analyses. The positive charges in $F_3S{\equiv}NXeF^+$ occur on Xe and S with the charge on Xe decreasing only slightly from 1.32 (1.33) in gas-phase XeF^+ to 1.29 (1.25) in $F_3S{\equiv}NXeF^+$. The small xenon valency increase from 0.47 (0.45) in XeF^+ to 0.62 (0.66) in the adduct cation is matched by the increase in the nitrogen valency from 1.57 (1.46) to 1.74 (1.69) and is indicative of a weak bonding interaction with nitrogen, which is corroborated by the low Xe−N bond order [0.24 (0.27)]. The negative charge on the fluorine atom of XeF^+ [−0.32 (−0.33)] increases upon adduct formation [−0.46 (−0.46)], consistent with a longer, more polar Xe−F bond (Table 2) and a correspondingly lower F valency and Xe−F bond order. Contraction of the S−F bonds in $F_3S{\equiv}NXeF^+$ is in accord with the increased S−F bond order and valency, and the greater difference between the S and F charges. Interestingly, the N atom has a greater negative charge in the cation [−1.09 (−1.04)] when compared with that in $N{\equiv}SF_3$ [−0.82 (−0.75)], with the negative charge increase on N being

(53) MacDougall, P. J.; Schrobilgen, G. J.; Bader, R. F. W. *Inorg. Chem.* **1989**, *28*, 763−769.

Table 4. Raman Vibrational Frequencies and Intensities for N≡SF_3 and [F_3S≡NXeF][AsF_6] and Calculated Vibrational Frequencies, Intensities, and Assignments for N≡SF_3, F_3S≡$NXeF^+$, and XeF^+ [a]

frequency, cm^{-1}							
N≡SF_3			F_3S≡$NXeF^+$				
	calcd[c]			calcd[c]		assignments	
exptl[b]	MP2	SVWN	exptl[b,d]	MP2	SVWN	F_3S≡$NXeF^+$ (C_1)	AsF_6^- (O_h)
1524 (7) 1519 (39) 1503 (3)	1503 [68] (16)	1466 [73] (9)	1548 (1) 1542 sh 1527 (10)	1619 [475] (84)	1607 [459] (86)	ν(SN)	
855 (3) 851 (13) 811 (7) 809 (5)	809 [211] (3)	751 [194] (5)	952 (4) 942 (4) 934 (1)	941 [193] (3)	924 [179] (4)	$\nu_{as}(SF_3)$	
779 (100)	759 [149] (23)	714 [122] (24)	876 (1) 875 (1) 869 (28)	873 [89] (36)	846 [98] (56)	$\nu_s(SF_3)$	
			724 sh 717 sh				$\nu_3(T_{1u})$
			701 (2) 689 (31)				$\nu_1(A_{1g})$
			594 (8) 580 (5)				$\nu_2(E_g)$
530 (10) 526 (2)	511 [27] (2)	443 [14] (2)	570 (22) 565 (21) 558 sh 556 sh	547 [10] (1)	518 [11] (1)	$\delta_s(SF_3)$	
			550 (100)	610 [98] (63)	604 [114] (44)	ν(XeF)	
445 (21) 438 (14)	419 [7] (4)	376 [6] (4)	471 (8) 448 (6)	440 [20] (4)	407 [16] (3)	$\delta(NSF_2)$	
			406 (3) 402 (2) 395 (2)				$\nu_4(T_{1u})$
			373 (6)				$\nu_5(T_{2g})$
355 (21) 349 (30)	337 [2] (4)	295 [1] (3)	369 (6) 357 (8)	345 [5] (3)	318 [5] (2)	$\delta_{as}(NSF_3)$	
			246 (1)				$\nu_6(T_{2u})$
			218 (3)				
			211 sh				
			206 (7)				
			194 (3)	161 [47] (1)	177 [31] (2)	ν(XeN)	
			177 (4)	175 [5] (1)	171 [5] (1)	δ(NXeF)	
			118 (1) br				
			95 (3)				
			n.o.	32 [<1] (1)	15 [<1] (1)	torsion about Xe	

[a] The calculated stretching frequency of gas-phase XeF^+ occurs at 665 (MP2) and 667 (SVWN) cm^{-1}. The experimental frequency of XeF^+ in its salts occurs at 608, 610 (AsF_6^-),[52] 615 (SbF_6^-),[37] 602, 608 (BiF_6^-),[38] 619 ($Sb_2F_{11}^-$),[37] and 605, 609 ($Bi_2F_{11}^-$) cm^{-1}.[38] [b] Values in parentheses denote experimental Raman intensities. [c] Infrared intensities (in km mol^{-1}) are given in brackets, calculated Raman intensities (in $Å^4$ amu^{-1}) are given in parentheses. [d] Abbreviations denote shoulder (sh), broad (br), and not observed (n.o.).

Table 5. Natural Bond Orbital (NBO) Charges, Valencies, and Bond Orders for F_3S≡$NXeF^+$, N≡SF_3, and XeF^+

	F_3S≡$NXeF^+$				N≡SF_3				XeF^+			
	charges		valencies		charges		valencies		charges		valencies	
atom	MP2	SVWN	MP2	SVWN	MP2	SVWN	MP2	SVWN	MP2	SVWN	MP2	SVWN
F_{Xe}	−0.46	−0.46	0.38	0.39					−0.32	−0.33	0.47	0.45
Xe	1.29	1.25	0.62	0.66					1.32	1.33	0.47	0.45
N	−1.09	−1.04	1.74	1.69	−0.82	−0.75	1.57	1.46				
S	2.45	2.35	3.84	3.62	2.19	2.06	3.68	3.34				
F_S	−0.40	−0.37	0.64	0.59	−0.46	−0.44	0.56	0.50				

bond orders

	F_3S≡$NXeF^+$		N≡SF_3		XeF^+	
bond	MP2	SVWN	MP2	SVWN	MP2	SVWN
F−Xe	0.38	0.39			0.47	0.45
Xe−N	0.24	0.27				
N−S	1.62	1.54	1.69	1.57		
S−F	0.74	0.69	0.66	0.59		

matched by the positive charge increase on S [N≡SF_3, 2.19 (2.06); F_3S≡$NXeF^+$, 2.45 (2.35)].

Among the plausible contributions to a valence bond description of F_3S≡$NXeF^+$ (structures I−X), the calculated

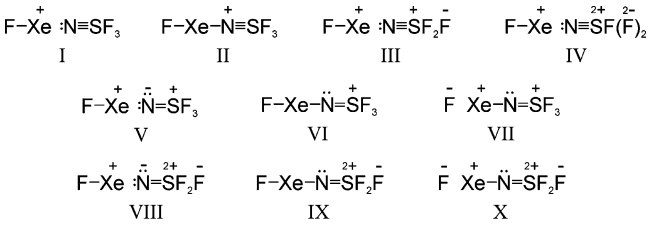

increase in electron density on N of the cation, relative to that of the free base, suggests that valence structures V and VIII are significant contributors. The negative charge on nitrogen in these structures is presumably stabilized, through polarization, by the positive charge on Xe. Structures V and VIII also account for the high positive charges on Xe and S and appear to best represent the calculated charge distributions. A prior computational study of $N{\equiv}SF_3$ concluded that any withdrawal of electron density from nitrogen results in significant stabilization of the S−N and S−F bonds and in their contraction.[54]

(c) Nature of the Xenon−Nitrogen Bond. The gas-phase reaction energies corresponding to xenon-ligand dissociation were calculated at the MP2 level of theory for $F_3S{\equiv}NXeF^+$, $HC{\equiv}NXeF^+$, and XeF_2 and are listed in Scheme 1. The donor−acceptor adduct dissociation energies of $F_3S{\equiv}NXeF^+$ and $HC{\equiv}NXeF^+$ are remarkably similar. These donor−acceptor interactions are decidedly weaker than those of the XeF^+ and $F^-/N(SO_2F)_2^-$ ions, but notably stronger than the As−N dissociation energies of $HC{\equiv}NAsF_5$ and $F_3S{\equiv}NAsF_5$. Under gas-phase conditions, it is clear that XeF^+ is a significantly stronger Lewis acid than AsF_5 toward both bases. These findings are consistent with a valence bond description of $F_3S{\equiv}NXeF^+$ that is dominated by the nonbonded structures V and VIII (vide supra) and with the spectroscopic and structural findings, i.e., correlations of Xe−F bond length and vibrational frequency with base strength,[37,53] placing the Xe−N interactions of $F_3S{\equiv}NXeF^+$ and $HC{\equiv}NXeF^+$ toward the most ionic end of the scale. The similar changes in XeF stretching frequencies and bond length for $HC{\equiv}N$ and $N{\equiv}SF_3$ upon complexation with XeF^+, as well as similar charge distribution changes for $HC{\equiv}N$ and $HC{\equiv}NXeF^+$,[53] yields a picture of adduct formation between XeF^+ and $N{\equiv}SF_3$ that is similar to that of XeF^+ and $HC{\equiv}N$. In this depiction, mutual penetration of outer diffuse nonbonded densities of the Xe and N atoms which, unlike a covalent interaction, produces no substantial shared density as reflected in the low Xe−N bond order and small changes in Xe and N valencies (Table 5). Instead, the final density and bond strength of the interaction are primarily determined by the extent of interpenetration of their closed shell densities, which leads to little modification of the Xe charge but polarization of, and increased negative charge on, the N donor atom (vide supra).

Scheme 1. Donor−Acceptor Adduct Dissociation Energies (kJ mol^{-1}) for Selected Species Calculated at the MP2/(SDB-)cc-pVTZ Level of Theory

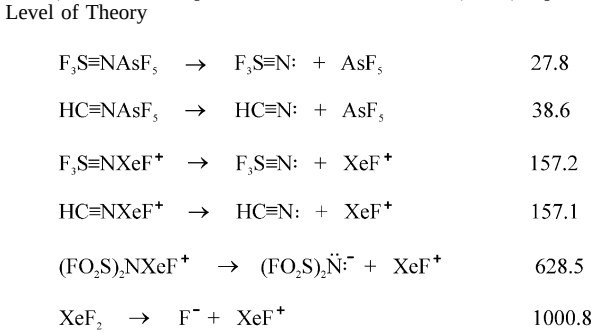

Conclusions

The synthesis and structural characterization of the $F_3S{\equiv}NXeF^+$ cation provides in addition to the $HC{\equiv}NXeF^+$ cation, a further example of xenon bound to a formally sp-hybridized nitrogen atom of an inorganic nitrogen base and affirms that $N{\equiv}SF_3$ is stable to oxidative attack by the highly electrophilic XeF^+ cation. Raman and NMR spectroscopic studies and an X-ray crystallographic study of $[F_3S{\equiv}NXeF][AsF_6]$ demonstrate that the $F_3S{\equiv}NXeF^+$ cation possesses among the longest Xe−N bonds known. This is corroborated by the deformation of the Xe−N−S angle from its linear gas-phase geometry to the severely bent arrangement that results from crystal packing in the solid-state structure of $[F_3S{\equiv}NXeF][AsF_6]$. These experimental findings, complimented by electronic structure calculations, reveal that $F_3S{\equiv}NXeF^+$ is among the weakest donor−acceptor adducts of XeF^+ and has an Xe−N donor−acceptor bond strength that is very similar to that of $HC{\equiv}NXeF^+$ but significantly greater than those of the AsF_5 adducts of $HC{\equiv}N$ and $N{\equiv}SF_3$. Despite the low dissociation energy of the donor−acceptor bond in $F_3S{\equiv}NXeF^+$, solution ^{129}Xe, ^{19}F, and ^{14}N NMR studies reveal that the $F_3S{\equiv}NXeF^+$ cation is nonlabile at low temperatures in HF and BrF_5 solvents.

Experimental Section

Apparatus and Materials. All manipulations were performed under anhydrous conditions as previously described.[55] Literature methods were used to prepare $N{\equiv}SF_3$[28] and $[XeF][AsF_6]$[37] and to purify HF (Harshaw Chemical Co.),[12] BrF_5 (Matheson),[56] and SO_2ClF (Allied Chemical).[57]

$[F_3S{\equiv}NXeF][AsF_6]$. In a typical synthesis, $[XeF][AsF_6]$ (0.1004 g, 0.2959 mmol) was loaded into a $^1/_4$-in. o.d. FEP tube, fitted with a Kel-F valve, and connected to an FEP submanifold that was, in turn, connected to a stainless steel cylinder containing $N{\equiv}SF_3$. The cylinder was fitted with two Whitey valves separated by a ca. 5-cm length of $^1/_4$-in o.d. stainless-steel tubing to produce an aliquot (ca. 1.4 mL) which was pressurized with $N{\equiv}SF_3$. Condensation of successive small-volume aliquots of gaseous $N{\equiv}SF_3$ allowed controlled metering of $N{\equiv}SF_3$ into the reaction vessel. Frozen $N{\equiv}SF_3$, which accumulated at the top of the reaction vessel at −196 °C, was warmed to −78 °C, whereupon it melted and reacted with $[XeF][AsF_6]$ on contact and warming (−25 to −15 °C). During the first hour, the solid changed from very pale yellow to white under a layer of liquid $N{\equiv}SF_3$. The reaction was allowed to proceed, with occasional mixing for ca. 6 h. The product and excess $N{\equiv}SF_3$ were then characterized by Raman spectroscopy to ensure that no unreacted $[XeF][AsF_6]$ remained. Excess $N{\equiv}SF_3$ was then

(54) Zirz, C.; Ahlrichs, R. *Inorg. Chem.* **1984**, *23*, 26−31.
(55) Casteel, W. J., Jr.; Dixon, D. A.; Mercier, H. P. A.; Schrobilgen, G. J. *Inorg. Chem.* **1996**, *35*, 4310−4322.
(56) Gillespie, R. J.; Schrobilgen, G. J. *Inorg. Chem.* **1976**, *15*, 22−31.
(57) Schrobilgen, G. J.; Holloway, J. H.; Granger, P.; Brevard, C. *Inorg. Chem.* **1978**, *17*, 980−987.

removed under dynamic vacuum at −50 °C, yielding a white powder, which was characterized by Raman spectroscopy and stored at −78 °C until it could be characterized by NMR spectroscopy or used for crystal growth.

Crystal Growth. Anhydrous HF (ca. 1 mL) was condensed onto [$F_3S{\equiv}NXeF][AsF_6$] (0.1309 g, 0.2959 mmol) at −196 °C that had been synthesized in situ in one arm of a $^1/_4$-in o.d. FEP T-shaped reactor fitted with a Kel-F valve. The reactor was warmed to −40 °C, to effect dissolution, and initially gave a colorless solution. While maintaining the reactor at −40 °C, it was attached to a vacuum line and pressurized to ca. 1 atm with dry nitrogen. The arm containing the solution was inclined at ca. 5° from horizontal inside the glass dewar of a crystal growing apparatus[58] that had been previously adjusted to −40 °C. The temperature was lowered over a period of 3 h to −45 °C, whereupon colorless crystals of [$F_3S{\equiv}NXeF][AsF_6$] began to grow on the walls of the FEP vessel as the supernatant changed to a very pale yellow color. The solution was then cooled, over a period of 30 min, to −55 °C where it was held for 30 min and then cooled over a period of 15 min to −60 °C where it was again held for a further 30 min to allow for more complete crystallization. Colorless, blade-shaped crystals were isolated by decanting the solvent under dry nitrogen into the side arm of the FEP vessel, which was immersed in liquid nitrogen, followed by evacuation and vacuum drying of the crystalline product under dynamic vacuum at −80 °C before the sidearm containing the supernatant was heat-sealed off. A crystal having the dimensions 0.32 × 0.18 × 0.10 mm^3 was selected at −105 ± 3 °C for low-temperature X-ray structure determination and was mounted in a cold stream (−173 °C) on a goniometer head as previously described.[59]

X-ray Crystallography. (a) Collection and Reduction of X-ray Data. The crystal was centered on a P4 Siemens diffractometer, equipped with a Siemens SMART 1K charge-coupled device (CCD) area detector that used the program SMART,[60] and a rotating anode using graphite-monochromated Mo Kα radiation ($\lambda = 0.71073$ Å). The diffraction data collection consisted of a full ψ rotation at $\chi = 0°$ using (1040 + 40) 0.36° frames, followed by a series of short (80 frames) ω scans at various ψ and χ settings to fill the gaps. The crystal-to-detector distance was 5.016 cm, and the data collection was carried out in a 512 × 512 pixel mode using 2 × 2 pixel binning. Processing was carried out by using the program SAINT,[60] which applied Lorentz and polarization corrections to three-dimensionally integrated diffraction spots. The program SADABS[61] was used for the scaling of diffraction data, the application of a decay correction, and an empirical absorption correction based on redundant reflections.

(b) Solution and Refinement of the Structures. The XPREP program was used to confirm the unit cell dimensions and the crystal lattice. The final refinement was obtained by introducing anisotropic parameters for all the atoms, an extinction parameter, and the recommended weight factor. The maximum electron densities in the final difference Fourier maps were located around the heavy atoms. All calculations were performed with the SHELXTL package for structure determination, refinement, and molecular graphics.[62] A solution was obtained by direct methods which located the Xe and As atoms. Successive difference Fourier syntheses revealed the positions of the fluorine, nitrogen, and sulfur atoms.

Nuclear Magnetic Resonance Spectroscopy. (a) NMR Sample Preparation. Samples of [$F_3S{\equiv}NXeF][AsF_6$] (ca. 0.050 g) were prepared in 4-mm o.d. FEP tubes fused to $^1/_4$-in. o.d. FEP tubes which were fitted with Kel-F valves. The samples were connected to an FEP submanifold that was, in turn, connected through a Kel-F valve to either a Kel-F vessel containing anhydrous HF or to an FEP vessel containing BrF_5 stored over anhydrous KF. The FEP submanifold was connected to a metal vacuum line, and ca. 0.5 mL of anhydrous HF or BrF_5 was statically distilled onto the salt at −196 °C. The NMR sample tubes were then heat-sealed under dynamic vacuum and stored at −196 °C until NMR spectra could be obtained. Samples were dissolved just prior to data acquisition at or below the temperature used to record their spectra. When obtaining low-temperature spectra, the 4-mm o.d. FEP tubes were inserted into a 5-mm o.d. thin wall precision glass NMR tube (Wilmad). A sample of $N{\equiv}SF_3$ was prepared by condensing $N{\equiv}SF_3$ into a precision 5-mm o.d. glass NMR tube at −196 °C, as described above, followed by condensation of SO_2ClF solvent and heat sealing the tube under dynamic vacuum at −196 °C.

(b) NMR Instrumentation and Spectral Acquisitions. Fluorine-19, ^{129}Xe, and ^{14}N NMR spectra were recorded unlocked (field drift <0.1 Hz h^{-1}) on a Bruker DRX-500 spectrometer equipped with an 11.744-T cryomagnet. The NMR probe was cooled using a nitrogen flow and variable-temperature controller (BV-T 3000).

The ^{19}F NMR spectra were acquired using a 5-mm combination $^1H/^{19}F$ probe operating at 470.592 MHz. The spectra were recorded in 32K memories, with spectral width settings of 24 kHz and acquisition times of 1.39 s, and were zero-filled to 64K, yielding data-point resolutions of 0.36 Hz/data point. Relaxation delays of 0.10 s were applied, and 1600 transients were accumulated.

The ^{129}Xe (^{14}N) NMR spectra were obtained using a 5-mm broadband inverse probe operating at 138.086 (36.141) MHz. The spectra were recorded in 32K memories, with spectral width settings of 97.1 (36.2) kHz and acquisition times of 0.17 (0.45) s, and were zero-filled to 64K, yielding data-point resolutions of 2.96 (1.10) Hz/data point. Relaxation delays of 0.10 (0) s were applied, and 32 000 (16 000) transients were accumulated.

Pulse widths, corresponding to bulk magnetization tip angles of ∼90°, were 6.0 (^{14}N), 8.5 (^{19}F) and 10.0 (^{129}Xe) μs. Line broadenings of 0.10 (^{19}F) and 5.0 (^{129}Xe and ^{14}N) Hz were used in the exponential multiplication of the free induction decays prior to Fourier transformation. In the case of the F-on-S environments of $F_3S{\equiv}NXeF^+$ (HF and BrF_5 solvents) and $N{\equiv}SF_3$ (SO_2ClF solvent), Gaussian multiplication was used to enhance spectral resolution.

The ^{14}N, ^{19}F, and ^{129}Xe spectra were referenced externally at 30 °C to samples of neat CH_3NO_2, $CFCl_3$, and $XeOF_4$, respectively. The chemical shift convention used is that a positive (negative) sign indicates a chemical shift to high (low) frequency of the reference compound.

Raman Spectroscopy. The low-temperature (−150 °C) Raman spectrum of [$F_3S{\equiv}NXeF][AsF_6$] was recorded on a Bruker RFS 100 FT Raman spectrometer using 1064-nm excitation and a resolution of 1 cm^{-1} as previously described.[63] The spectrum was recorded using a laser power of 350 mW, and a total of 1600 scans were acquired.

Computational Methods. Electronic structure calculations were carried out at the MP2 and SVWN (DFT) levels of theory using

(58) Lehmann, J. F.; Dixon, D. A.; Schrobilgen, G. J. *Inorg. Chem.* **2001**, *40*, 3002−3017.
(59) Gerken, M.; Dixon, D. A.; Schrobilgen, G. J. *Inorg. Chem.* **2000**, *39*, 4244−4255.
(60) *SMART*, release 5.611, and *SAINT*, release 6.02; Siemens Energy and Automation Inc.; Madison, WI, 1999.
(61) Sheldrick, G. M. *SADABS (Siemens Area Detector Absorption Corrections), version 2.03*; Siemens Analytical X-ray Instruments, Inc.: Madison, WI, 1999.
(62) Sheldrick, G. M. *SHELXTL-Plus*, release 5.1; Siemens Analytical X-ray Instruments, Inc.; Madison, WI, 1998.
(63) Casteel, W. J., Jr.; Kolb, P.; LeBlond, N.; Mercier, H. P. A.; Schrobilgen, G. J. *Inorg. Chem.* **1996**, *35*, 929−942.

the program Gaussian 03[64] for geometry optimizations and vibrational frequencies and intensities for the $F_3S{\equiv}NXeF^+$ cation. The standard all-electron cc-pVTZ basis set, as implemented in the Gaussian program, was utilized for all elements except Xe, for which the semirelativistic large core (RLC) pseudopotential basis set SDB-cc-pVTZ was used.[65] The combined use of cc-pVTZ and SDB-cc-pVTZ basis sets is indicated by (SDB-)cc-pVTZ. The program GaussView[66] was used to visualize the vibrational displacements that form the basis of the vibrational mode descriptions given in Table 4.

Acknowledgment. This paper is dedicated to our friend and colleague, Professor Neil Bartlett, on the occasion of his 75th birthday and in recognition of his many outstanding contributions across a broad spectrum of fluorine chemistry. We thank the Natural Sciences and Engineering Research Council (NSERC) of Canada for financial support in the form of a research grant (G.J.S.), the Ontario Ministry of Training, Colleges and Universities for the award of graduate scholarships (G.L.S.), and the computational resources provided by SHARCNet (Shared Hierarchical Academic Research Computing Network; www.sharcnet.ca).

Supporting Information Available: Correlation diagrams for the vibrational modes of $[F_3S{\equiv}NXeF][AsF_6]$ (Table S1) and an X-ray crystallographic file in CIF format for the structure determination of $[F_3S{\equiv}NXeF][AsF_6]$. This material is available free of charge via the Internet at http://pubs.acs.org.

IC061899+

(64) Frisch, M. J.; Trucks, G. W.; Schlegel, H. B.; Scuseria, G. E.; Robb, M. A.; Cheeseman, J. R.; Zakrzewski, V. G.; Montgomery, J. A., Jr.; Stratmann, R. E.; Burant, J. C.; Dapprich, S.; Millam, J. M.; Daniels, A. D.; Kudin, K. N.; Strain, M. C.; Farkas, O.; Tomasi, J.; Barone, V.; Cossi, M.; Cammi, R.; Mennucci, B.; Pomelli, C.; Adamo, C.; Clifford, S.; Ochterski, J.; Petersson, G. A.; Ayala, P. Y.; Cui, Q.; Morokuma, K.; Malick, D. K.; Rabuck, A. D.; Raghavachari, K.; Foresman, J. B.; Cioslowski, J.; Ortiz, J. V.; Stefanov, B. B.; Liu, G.; Liashenko, A.; Piskorz, P.; Komaromi, I.; Gomperts, R.; Martin, R. L.; Fox, D. J.; Keith, T.; Al-Laham, M. A.; Peng, C. Y.; Nanayakkara, A.; Gonzalez, C.; Challacombe, M.; Gill, P. M. W.; Johnson, B. G.; Chen, W.; Wong, M. W.; Andres, J. L.; Head-Gordon, M.; Replogle, E. S.; Pople, J. A. *Gaussian 98*, revision A.11; Gaussian, Inc.: Pittsburgh, PA, 1998.

(65) Basis sets were obtained from the Extensible Computational Chemistry Environment Basis set Database, version 2/25/04, as developed and distributed by the Molecular Science Computing Facility, Environmental and Molecular Science Laboratory, which is part of the Pacific Northwest Laboratory, P.O. Box 999, Richland, WA 99352.

(66) *GaussView*, release 3.0; Gaussian Inc.: Pittsburgh, PA, 2003.